Automated 3D quantitative assessment and measurement of alpha angles from the femoral head-neck junction using MR imaging

IOP Publishing | Institute of Physics and Engineering in Medicine Physics in Medicine & Biology

Phys. Med. Biol. **60** (2015) 7601–7616 doi:10.1088/0031-9155/60/19/7601

Automated 3D quantitative assessment and measurement of alpha angles from the femoral head-neck junction using MR imaging

Ying Xia[1,2], Jurgen Fripp[2], Shekhar S Chandra[1,2] Duncan Walker[3], Stuart Crozier[1] and Craig Engstrom[4]

[1] School of Information Technology and Electrical Engineering, The University of Queensland, St. Lucia, QLD 4027, Australia
[2] Australian e-Health Research Centre, CSIRO, Brisbane QLD 4029, Australia
[3] Wesley Medical Imaging, Brisbane QLD 4066, Australia
[4] School of Human Movements Studies, The University of Queensland, St. Lucia, QLD 4027, Australia

E-mail: ying.xia@uqconnect.edu.au

Received 1 April 2015, revised 14 July 2015
Accepted for publication 14 August 2015
Published 21 September 2015

Abstract

To develop an automated approach for 3D quantitative assessment and measurement of alpha angles from the femoral head-neck (FHN) junction using bone models derived from magnetic resonance (MR) images of the hip joint.

Bilateral MR images of the hip joints were acquired from 30 male volunteers (healthy active individuals and high-performance athletes, aged 18–49 years) using a water-excited 3D dual echo steady state (DESS) sequence. In a subset of these subjects (18 water-polo players), additional True Fast Imaging with Steady-state Precession (TrueFISP) images were acquired from the right hip joint. For both MR image sets, an active shape model based algorithm was used to generate automated 3D bone reconstructions of the proximal femur. Subsequently, a local coordinate system of the femur was constructed to compute a 2D shape map to project femoral head sphericity for calculation of alpha angles around the FHN junction. To evaluate automated alpha angle measures, manual analyses were performed on anterosuperior and anterior radial MR slices from the FHN junction that were automatically reformatted using the constructed coordinate system.

High intra- and inter-rater reliability (intra-class correlation coefficients > 0.95) was found for manual alpha angle measurements from the auto-extracted anterosuperior and anterior radial slices. Strong correlations

were observed between manual and automatic measures of alpha angles for anterosuperior ($r = 0.84$) and anterior ($r = 0.92$) FHN positions. For matched DESS and TrueFISP images, there were no significant differences between automated alpha angle measures obtained from the upper anterior quadrant of the FHN junction (two-way repeated measures ANOVA, $F < 0.01$, $p = 0.98$).

Our automatic 3D method analysed MR images of the hip joints to generate alpha angle measures around the FHN junction circumference with very good reliability and reproducibility. This work has the potential to improve analyses of cam-type lesions of the FHN junction for large-scale morphometric and clinical MR investigations of the human hip region.

Keywords: alpha angle, femoroacetabular impingement, magnetic resonance imaging, cam lesion, hip joint, quantitative assessment

(Some figures may appear in colour only in the online journal)

1. Introduction

Symptomatic cam-type femoroacetabular impingement (FAI) is frequently associated with bone exostosis of the femoral head-neck (FHN) junction which impact upon the acetabular labrum and cartilage particularly during flexion and internal rotation of the hip joint (Tannast *et al* 2007, Streit *et al* 2012, Aliprandi *et al* 2014). Cam lesions have been suggested to alter hip joint loading, which predisposes to labral and cartilage damage at the anterosuperior acetabular rim due to abnormal shear and compressive forces that may lead to degenerative joint disease (Wagner *et al* 2003, Tannast *et al* 2008). Accordingly, the detection and accurate quantification of cam lesions, as a proposed risk factor in the development of hip osteoarthritis (OA) (Ganz *et al* 2003, Tannast *et al* 2008), is important for clinical investigations and evaluation of treatments focusing on modifying the course of hip OA.

Traditionally, standard radiographs (x-rays) have been used to diagnose cam-type FAI involving bony deformities at the FHN junction (Meyer *et al* 2006). Cam lesion severity is frequently assessed using a two-dimensional (2D) alpha angle (Nötzli *et al* 2002). A value exceeding 50° is commonly used as an indicator of femoral head asphericity and irregularity of the FHN junction (Tannast *et al* 2007). However, alpha angle measures from planar x-ray images of the proximal femur have proven limitations in depicting the severity of cam lesions given the variable three-dimensional (3D) morphology and location of these bone deformities (Meyer *et al* 2006, Clohisy *et al* 2009, Dudda *et al* 2009, Barton *et al* 2011). Meyer *et al* (2006) reported that femoral head asphericity (based on alpha angle data) was likely to be underestimated from routine anteroposterior radiographs. Radiographic diagnosis of cam-type FAI also had low intra- and inter-observer agreement (Cohen's kappa coefficients <0.6) with structural features (e.g. head sphericity, head-neck offset/junction) (Clohisy *et al* 2009).

Computed tomography (CT) and magnetic resonance (MR) imaging provide volumetric data acquisition and multiplanar reconstruction allowing detailed 3D assessments of bone morphology at the FHN junction for enhanced measurement of cam lesions (Bedi *et al* 2012). In recent CT-based studies, 3D bone reconstructions of the proximal femur have been used for evaluation of femoral head sphericity using alpha angle measures from radial plane images (Beaulé *et al* 2005, Audenaert *et al* 2011) and model fitting (e.g. sphere, conchoid) (Harris *et al* 2013a, Masjedi *et al* 2013a). Principal component analysis (PCA) modelling has also been employed to investigate 3D shape variations in bone morphology around the FHN junction (Harris *et al* 2013b). In a patented method, Chabanas *et al* (2014) used an automatic approach

based around 3D surface models to determine the contour of the FHN junction and identify the location of cam lesions from CT images.

In MR imaging, manual or semi-automated selection and analysis of slices through the FHN junction obtained in one or several reformatted 2D planes is normally used for the assessment of cam lesions (Nötzli *et al* 2002, Rakhra *et al* 2009). Sutter *et al* (2012) used radially reformatted MR images of the proximal femur for detecting the presence of cam lesions at the anterosuperior FHN junction and found a 60° alpha angle diagnostic cut-off value (sensitivity and specificity ~70%) between symptomatic FAI patients and asymptomatic volunteers. However, alpha angle measurement derived from a limited number of reconstructed 2D planes does not fully evaluate the 3D morphology of the FHN junction, particularly given the variable presentation characteristics of cam lesions (Rakhra *et al* 2009). Recently, Kang *et al* (2013) assessed the entire circumference of the FHN junction using 2D diagnostic graphs derived from manual bone reconstructions of high-resolution T1w dual sense spin echo images, which yielded good discrimination between FAI patients ($N = 5$) and asymptomatic volunteers ($N = 4$). Therefore, the development of a 3D MR-based method for direct visualization and quantitative descriptions of the 3D bone morphology of the FHN junction would be extremely beneficial for detailed analyses of cam lesions including evaluation of the magnitude/extent and epicentre of these bone protrusions. The automatic provision of reliable and reproducible quantitative morphological data (e.g. full circumferential alpha angles) would facilitate large-scale research and clinical studies on cam FAI.

Here, we present a novel automated method for analysis of MR images of the hip joint based on our bone segmentation algorithm (Xia *et al* 2013) that allows 3D reconstruction of the proximal femur to determine FHN morphometric data and 360° calculation of alpha angles. In this paper, the automated measurement of alpha angles is validated against manual measures obtained from bilateral DESS images of the hip joints. Additionally, analyses of automated 3D reconstructions of the proximal femur and alpha angle measurements from paired DESS and True Fast Imaging with Steady-state Precession (TrueFISP) examinations are compared to assess the performance of our approach for MR images with different contrast characteristics.

2. Materials and methods

2.1. MR image datasets and acquisition protocols

Bilateral MR images of the hip joints were acquired from 30 male volunteers (including healthy active individuals and high-performance athletes without a history of developmental hip disorders, aged 18–49 years, body mass index $25.9 \pm 2.6\,\mathrm{kg\,m^{-2}}$) using a 3D water-excited DESS sequence. In a subset of these volunteers (18 water-polo players), additional unilateral 3D TrueFISP images were acquired from the right hip joint. The MR imaging was performed using a 3T MR scanner (Magnetom Trio; Siemens, Germany). A large 4-channel body matrix, with Generalized Autocalibrating Partially Parallel Acquisition (GRAPPA) (×2) enabled, was used for image acquisition. The bilateral DESS scans were obtained with a large field of view (FOV) using the following parameters: TR/TE: 15.46/5.16 ms, flip angle: 25°, slice thickness: 0.610 mm, FOV: $38.6 \times 24.1\,\mathrm{cm^2}$, image matrix: 576×360 and in-plane spacing: 0.670 mm. The TrueFISP examinations were obtained using a small FOV centred over the right hip joint with the following parameters: TR/TE: 10.65/4.46 ms, flip angle: 30°, slice thickness: 0.490 mm, FOV: $15 \times 15\,\mathrm{cm^2}$, image matrix: 320×320 and in-plane spacing: 0.468 mm. Slice interpolation (K-space) was enabled in the unilateral TrueFISP scans to obtain an in-plane resolution of 0.234 mm. Example coronal slices are presented in figure 1 to illustrate the different

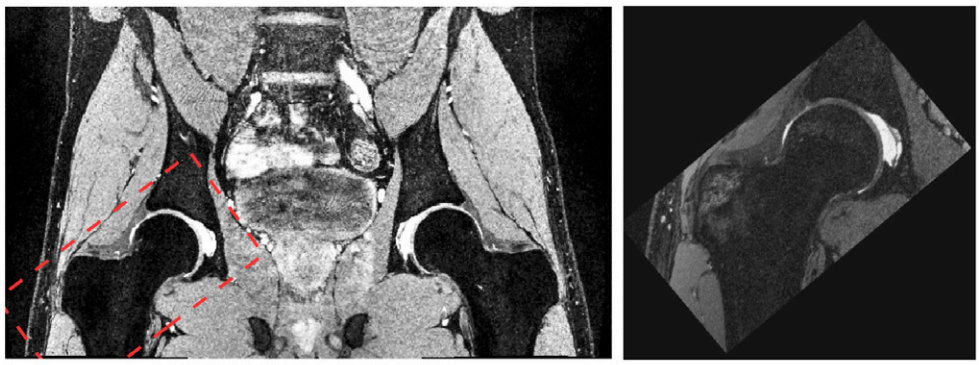

Figure 1. Example coronal slices of the paired (a) bilateral DESS and (b) unilateral TrueFISP images acquired from the same subject. The red rectangle indicates a smaller acquisition FOV used for the TrueFISP examination for the right-side hip joint.

FOV coverage of the hip region between these two acquisition protocols. The medical research ethics committee of the University of Queensland approved the current study. Informed written consent was obtained from all participants involved in the research.

2.2. Manual alpha angle measurements

Manual measurements (ground truth) of alpha angles were performed on all 30 DESS (bilateral) examinations by two raters: an experienced radiologist (Rater 1) and an experienced anatomist (Rater 2). From the 3D images of each hip joint, image reformation was automatically performed using our proposed method (described below) to generate images from a series of radial plane slices to provide standardized (Rater independent) visualization of bone morphology for dedicated analyses in the upper anterior quadrant of the FHN junction. Both raters considered the auto-extracted radial slices to be consistent with manually reformatted images they had analysed during previous clinical studies. Following the method of Nötzli *et al* (2002), alpha angles were manually measured from two reformatted, auto-extracted radial slices: anterosuperior—45° and anterior—90° images (figure 2). A plugin developed from our inhouse SMILI (Simple Medical Imaging Library Interface)[5] package (Chandra *et al* 2015a, Chandra *et al* 2015b) was used for all the preceding processes.

In the dataset of bilateral DESS images, the intra-rater (Rater 2) and inter-rater reliability for alpha angle measurements was determined for both the anterosuperior and anterior radial plane slices. All manual measurements were performed in a blinded fashion. The larger alpha angle from the two repeated measures of Rater 2 for each hip and both radial planes was used for comparison with the corresponding automatic measures in the present study.

2.3. Automated MR-based 3D bone reconstruction and alpha angle measurements

The full workflow diagram for automated extraction of the 3D bone morphology of the proximal femur and measurement of alpha angles for assessment of cam-type lesions involves: the active shape model (ASM) based bone segmentation pipeline (Xia *et al* 2013), construction of a 3D local coordinate system (figure 3(a)), automatic MR image reformation (figure 3(b)) and alpha angle measurement (figure 3(c)).

[5] Available at http://smili-project.sourceforge.net

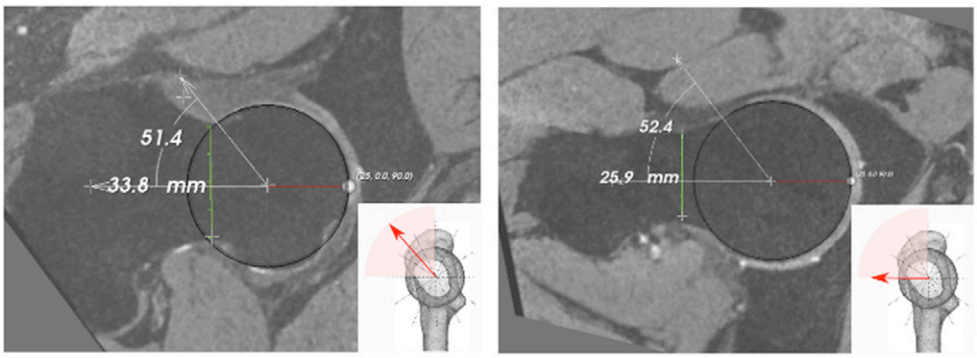

Figure 2. Example manual alpha angle measurements for the (a) anterosuperior and (b) anterior positions of the FHN junction from auto-extracted 2D radial planes reformatted from bilateral DESS images.

2.3.1. Automatic bone segmentation. In a pre-processing step, the bone surface of the proximal femur was automatically segmented from MR images using a 3D ASM-based method (Xia *et al* 2013). In brief, the automatic bone segmentation approach was applied to MR images of the hip region and consisted of (i) model initialization using a joint locator (Nishii *et al* 2004), (ii) coarse bone segmentation using composite statistical shape models (SSM) of the bone elements of the hip joint: a bilateral hip SSM (only for MR images encompassing bilateral hip joints) and SSMs of an individual hip joint, (iii) bone segmentation refinement using SSMs of an individual bone element (proximal femur, os coxa) and (iv) bone surface relaxation without shape constraints. A further improvement to the above segmentation method involved, before bone surface relaxation, additional refinement of the segmentation of the proximal femur using a focused SSM of the femur (Chandra *et al* 2014), which was built from the same training data but with pre-determined weights representing a specified region of interest (ROI) corresponding to the FHN junction. This focused shape model provided lower reconstruction errors and higher segmentation accuracy for the selected ROI in this portion of the femur.

2.3.2. Automatic 3D reference coordinate system construction. Based on the segmented 3D bone surfaces of the femur, a point landmark for the femoral head centre (FHC) and two reference axes (femoral neck (FN) and femoral shaft (FS) axes) were automatically determined based on sample points within the ROIs of the femoral head, neck and proximal shaft of the femur, respectively (i.e. pre-defined in the atlas surface of the proximal femur shown in figure 3), for construction of a new local reference coordinate system.

- The FHC was initialized using the Hough transform (Nishii *et al* 2004) applied to MR images followed by an iterative least-square algorithm for 3D sphere fitting to the femoral head of the segmented bone model (the pre-defined ROI of 'Fh' in figure 3(a)).
- The FN axis was determined as the central axis of an optimal one-sheeted hyperboloidal surface model (Masjedi *et al* 2013a, Sholukha *et al* 2011), which was best fitted to the 3D point cloud of the femoral neck that was the pre-defined ROI 'Fn' in figure 3(a) in the atlas model of the proximal femur. A random sample consensus paradigm (Fischler and Bolles 1981) integrated with the least-square-based quadric surface fitting algorithm (Dai *et al* 2007) was applied to estimate geometric parameters of this hyperboloid model and,

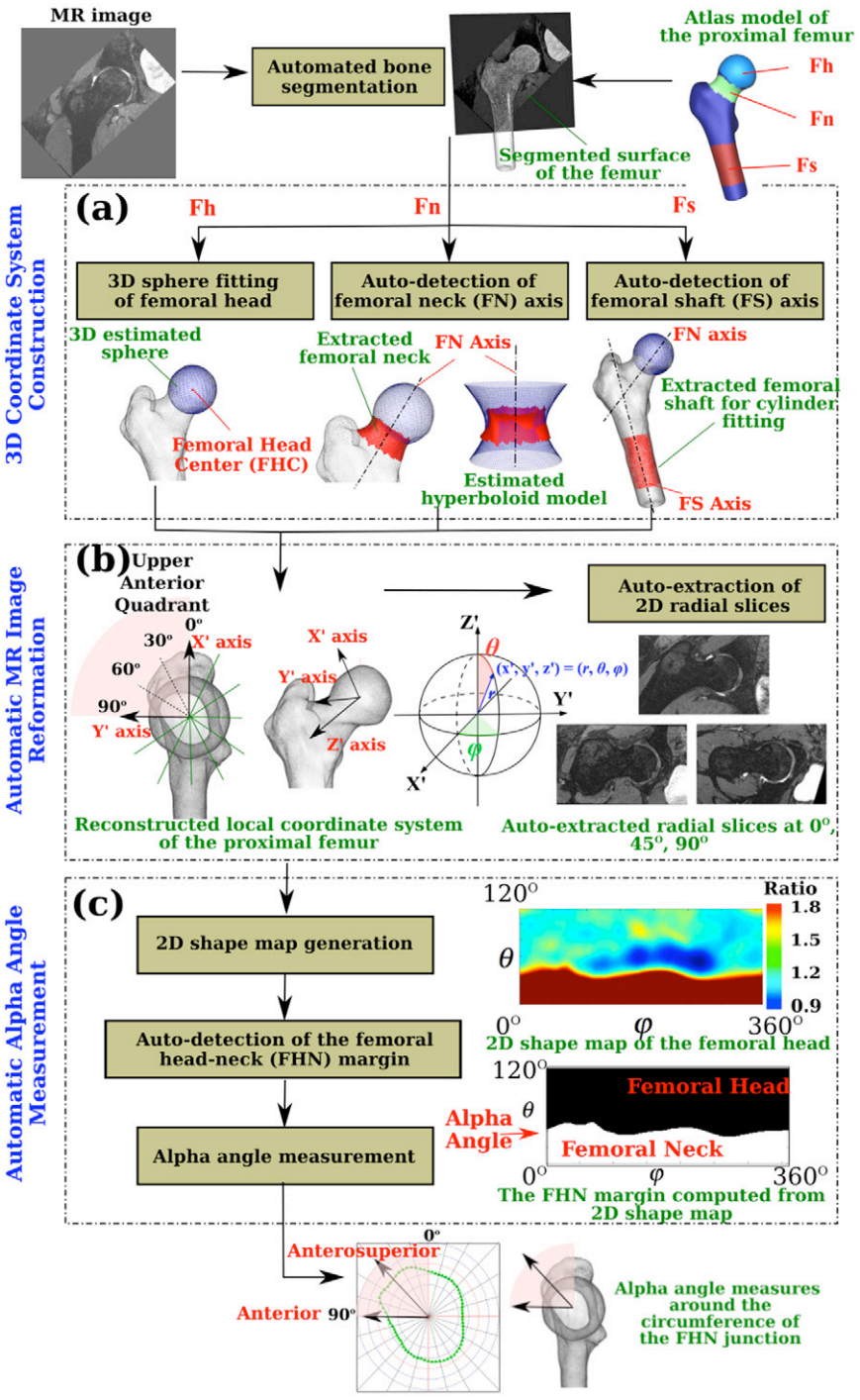

Figure 3. Workflow diagram of automated alpha angle measurement scheme for assessment of cam lesions from MR images of the hip joint.

simultaneously, to handle a major portion of outliers in the comparatively large number of sample points at the femoral neck.

- The FS axis was estimated by fitting an optimal elliptic cylinder model to the partial surface of the proximal femoral shaft (the ROI of 'Fs' in figure 3(a)).

Based on the detected FHC, FN and FS axes, the segmented bone surface of the proximal femur was rigidly transformed to a local 3D reference coordinate system (x', y', z') with the FHC as its origin. As illustrated in figure 3(b), the Z' axis was defined by the FN axis with its positive direction pointing towards the greater trochanter of the femur. The Y' axis was along the normal direction of the 2D plane determined by the axes of FN and FS and pointing anteriorly and the X' axis was aligned orthogonal to the resulting Y' and Z' axes and pointing superiorly. Each point (x', y', z') was expressed using spherical coordinates (r, θ, φ), where r, θ and φ denoted the radius, inclination angle and azimuth angle of this point, respectively.

With the constructed reference coordinate system, the MR images were automatically reformatted into a series of standardized radial 2D slices centred at the FHC and rotated around the FN axis. This emulated the manual reformation process commonly performed in previous studies (Sutter *et al* 2012, Zilkens *et al* 2013).

2.3.3. Automatic alpha angle measurement. Based on the local spherical coordinates (r, θ, φ), a 2D shape map, following the work of Kang *et al* (2013), was generated to assess the sphericity of the femoral head, where radial distances d_R from the FHC to the points of intersection with the bone surface of the femoral head were calculated and represented as a function of θ and φ. The generated 2D shape map (figure 3(c)) was a 120-by-360 matrix used to describe the 3D surface of the femoral head and neck, in which each element denoted a direction from the FHC as a coordinate pair (θ, φ), where $\theta = 1°, 2°, ..., 120°$ and $\varphi = 1°, 2°, ..., 360°$, and the intensity of each pixel was calculated as $I(\theta, \varphi) = d_R/R$, where R was the radius of the fitted sphere model.

With the computed 2D shape map of the femoral head, the FHN margin (figure 3(c)) was automatically located by finding a horizontal cut of the shape map with smoothness constraints allowing a maximum change of 1° between neighbouring columns. Thereafter, alpha angles for all the radial positions 1° ~ 360° (i.e. the entire circumference) of the FHN junction, were calculated for identification of cam lesions with reference to alpha angle measures as well as provision of data on the location (e.g. the epicentre) and size (e.g. extent of exostosis) of abnormal bone protrusion around the FHN junction.

2.3.4. Automated workflow time. For the bilateral DESS images, the entire automatic processing and measurement steps took around 13–14 min for an MR examination from one individual case using a normal PC (quad-core 2.53 GHz, 12 GB RAM). The majority of this time (i.e. ~12 min) was spent on bone segmentation (Xia *et al* 2013), from which the 3D femoral coordinate system and alpha angles around the entire circumference of the FHN junction were obtained. A similar computation time (<15 min) was required for automated analyses of the higher resolution unilateral TrueFISP images.

2.4. Validation method and statistical analyses

The validation of the bone segmentation was assessed using Dice's similarity coefficient (DSC) scores (Dice 1945) and mean absolute surface distance (MASD) values (Gerig *et al* 2001). The DSC score represents a spatial overlap (volume) index between the manual (ground truth) and automatic segmentations calculated as $DSC = 2N_{TP}/(2N_{TP} + N_{FP} + N_{FN})$,

where N_{TP}, N_{FP} and N_{FN} respectively denote true positive, false positive and false negative voxel counts. The MASD (in mm) is defined as:

$$d_{MASD} = [d_{avg}(S_A, S_M) + d_{avg}(S_M, S_A)]/2,$$

where $d_{avg}(S_A, S_M)$ is the average directed surface distance from all points on the automatic surface S_A to the manual surface S_M.

To visualize the distribution of segmentation errors locally at specific ROIs (i.e. the femoral head and neck), directed Hausdorff distances $d_{Hausdorff}$ (S_A, S_M) (Commandeur *et al* 2011) were presented in this study, which are defined as:

$$d_{Hausdorff}(S_A, S_M) = \max\{d(v_A, S_M), v_A \in S_A\},$$

where S_A and S_M are automatic and manual segmentation surfaces, respectively. Further, biases of the 3D coordinate systems constructed from MR images using the different DESS and TrueFISP acquisition sequences were compared using root mean square (RMS) errors (mm) for the FHC and angular differences (degrees) for the FN and FS axes.

All statistical analyses were performed using the R statistical package and $p < 0.05$ was set as an *a priori* significance level in the current study. The intra-class correlation coefficient (ICC), with 95% confidence intervals (CI), was used to evaluate the intra- and inter-rater reliability of manual alpha angle measures. The agreement between manual and automatic alpha angle measurements was assessed using linear regression and Pearson's correlation coefficients, with categorization of significant values of $r = 0.60$–0.79 as strong and 0.80–1 as very strong correlations (Harris *et al* 2014). Bland–Altman plots (Bland and Altman 1986) were used to visualize the agreement in alpha angle measures between the manual and automatic approaches. In terms of comparing the automated measures between the paired DESS and TrueFISP datasets, a two-way repeated measures ANOVA was performed using alpha angle data obtained at 4 positions in the upper anterior quadrant of the FHN junction.

3. Results

For all 3D bilateral DESS and unilateral TrueFISP examinations, the automatic scheme provided successful segmentations of the proximal femur allowing 360° measurement of alpha angles around the FHN junction. No user-interaction was required for any of the automatic segmentation and quantification steps or for any *post-hoc* manual editing of the resulting bone surfaces and alpha angle measures.

3.1. Intra- and inter-rater reliability of manual alpha angle measures from auto-extracted slices

The intra-rater reliability (Rater 2) for manual measurement of alpha angles from the auto-extracted reformatted radial slices from the DESS images was very high for both the anterosuperior (ICC(1,1) = 0.98; 95% CI: 0.96–0.99, $p < 0.01$) and anterior positions (ICC(1,1) = 0.97; 95% CI: 0.95–0.98, $p < 0.01$). Likewise, the inter-rater reliability for manual measurement of alpha angles from these auto-extracted radial DESS slices was very high for both the anterosuperior (ICC(2,1) = 0.95; 95% CI: 0.91–0.97, $p < 0.01$) and anterior positions (ICC(2,1) = 0.96; 95% CI: 0.94–0.98, $p < 0.01$). Linear regressions for the manual alpha angle data obtained by the Raters revealed very small biases of $-0.94° \pm 3.50°$ and $0.12° \pm 3.50°$ for the measures from the anterosuperior and anterior radial plane slices with very strong correlations of $r = 0.96$ and 0.95 ($p < 0.01$), respectively.

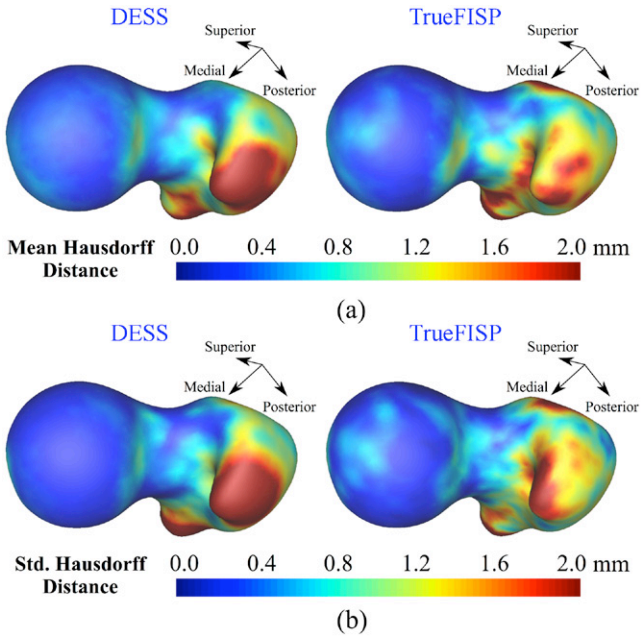

Figure 4. (a) Mean and (b) standard deviation maps of directed Hausdorff distance computed from validation results of the bilateral DESS ($N = 30$) and unilateral TrueFISP ($N = 18$) examinations.

3.2. Comparisons between manual (ground truth) and automatic measures

3.2.1. Bone reconstruction. Automatic bone reconstructions of the proximal femur obtained from the DESS images were validated against the corresponding manual segmentations reported in our previous work (Xia *et al* 2013). It achieved MASD and DSC values of 0.80 ± 0.21 mm and 0.95 ± 0.01, respectively, which compared favourably with the intra- and inter-rater reliability for manual bone segmentations of the proximal femur having mean DSC scores ~0.97 (Xia *et al* 2013). For the TrueFISP images, the corresponding DSC and MASD values between the manual and automatic segmentations were 0.95 ± 0.01 and 0.99 ± 0.19 mm, respectively. The mean and standard deviation (SD) of the directed Hausdorff distances are shown in figure 4 to illustrate the accuracy of the segmented femur surfaces, particularly at the femoral head and neck, and view the distribution of segmentation errors across various anatomical regions. The average Hausdorff distance for the femoral head and neck was under 0.8 mm with a very small variance, which indicates accurate bone delineation within this region achieved by the automatic segmentation scheme.

3.2.2. Alpha angle measurements. There were very strong positive, statistically significant correlations between the manual and automatic alpha angle measures obtained from the DESS images for both the anterosuperior ($r = 0.84$, $p < 0.01$) and anterior ($r = 0.92$, $p < 0.01$) positions (figures 5(a) and (b)). Bland–Altman plots (figures 5(c) and (d)) indicated average angular differences of $-2.49°$ (SD: 7.34°) and $-4.01°$ (SD: 3.98°) between the manual and automatic alpha angle measurements at the anterosuperior and anterior positions of the FHN junction, respectively. In figure 5(a), the extreme outlier was related to a focal ossification within the anterosuperior femoral cartilage observed by both raters (manual alpha angles ~80°) but no definitive bony protrusion (automatic alpha angle ~40°).

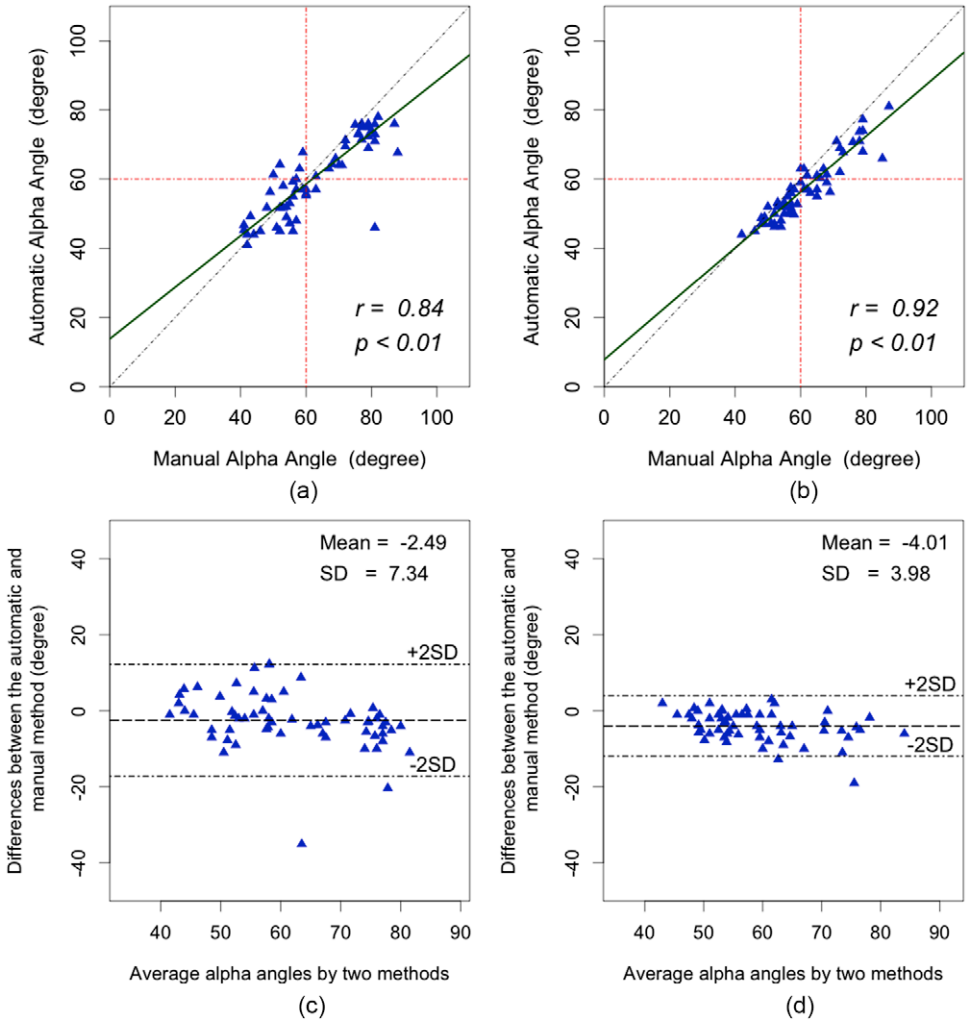

Figure 5. Statistical analyses of alpha angles at the positions of (a, c) 45° and (b, d) 90° of the FHN junction measured between the manual method based on automatic image reformation process and the proposed automatic assessment scheme from 30 bilateral DESS images: (a) and (b) are the scatter plots with the regression lines (*r* is the Pearson's correlation coefficient), (c) and (d) are the Bland–Altman plots.

3.3. Comparisons between automatic measures of alpha angles from DESS and TrueFISP images

Comparisons of the constructed coordinate systems using automated bone segmentations from the matched 3D DESS and TrueFISP scans (18 individuals, right hips) showed a mean RMS error of 0.83 mm (SD: 0.72 mm) for the FHC location and mean angular differences of 2.11° (SD: 0.94°) and 0.43° (SD: 0.49°) for the FN and FS axes, respectively. Figure 6 shows representative examples of the reformatted 2D radial plane slices at four different positions within the upper anterior quadrant of the FHN junction extracted from DESS and TrueFISP scans in cases having larger alpha angles (e.g. >60°) consistent with cam-type lesions and smaller alpha angles (e.g. <50°) without cam-type lesions. Figure 6 also illustrates that

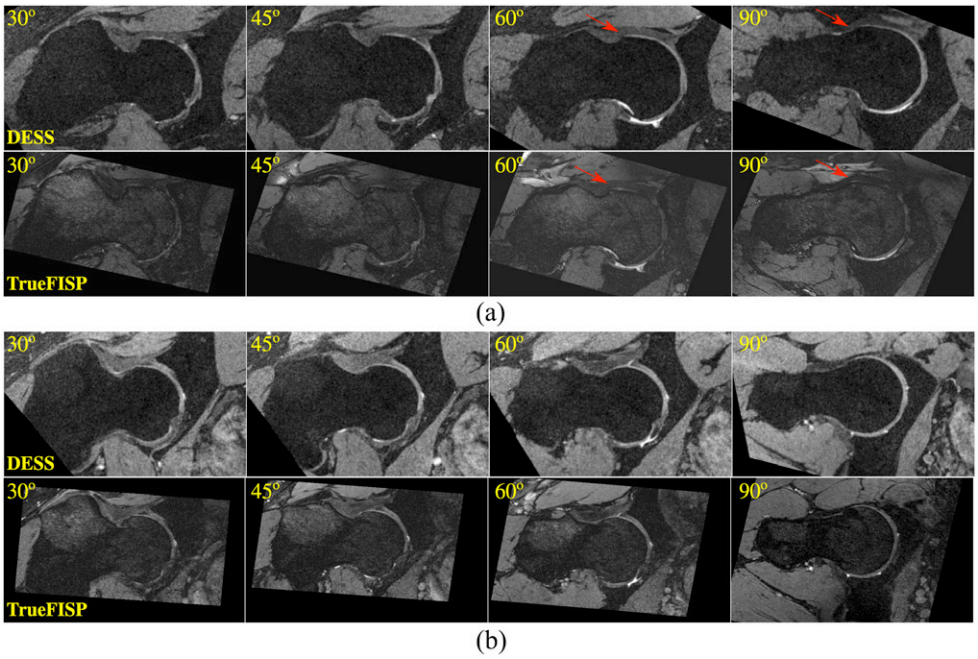

Figure 6. Representative auto-extracted 2D radial slices at four different positions in the upper anterior quadrant of the FHN junction (from left to right, 30°, 45°, 60°, 90°) from (top) DESS and (bottom) TrueFISP examinations of the right hip joints with (a) big and (b) small alpha angles (red arrows indicating the perceptible cam-type lesion).

despite differences in the contrast characteristics between the DESS and TrueFISP images, the automatic image reformation process is consistent using 3D local reference coordinates derived from the related automatic bone reconstructions of the proximal femur.

Figure 7(a) shows the mean (±95% CI) alpha angle curves computed from the automatic measures between the DESS and TrueFISP images. There was good agreement of alpha angles across all the locations 1° ~ 180° of the FHN junction obtained using our method, where the largest alpha angle was likely to be located within the upper anterior quadrant between 45° and 75° positions of the FHN junction. In figure 7(b), for four different pre-selected positions corresponding to 30°, 45°, 60° and 90°, there were strong correlations with Pearson's correlation coefficients $r = 0.86, 0.78, 0.83$ and 0.94 ($p < 0.01$) achieved between alpha angle measures from these two MR sequences. The two-way repeated measures ANOVA test showed no significant effects for MR sequence (i.e. DESS and TrueFISP) on the automatic alpha angle measures ($F < 0.01$, $p = 0.98$), although, as anatomically expected, there was a strong main effect for measurement position ($F = 14.36$, $p < 0.01$). There was no significant interaction between MR sequence and measurement positions of the FHN junction ($F = 1.5$, $p = 0.21$).

4. Discussion

We have successfully developed a quantitative assessment method for analyses of MR images of the hip joint that automatically evaluates 3D bone morphology and provides 360° calculation of alpha angles around the FHN junction. At the anterosuperior and anterior FHN positions, as investigated in previous clinical studies (Pfirrmann *et al* 2006, Dudda *et al* 2009,

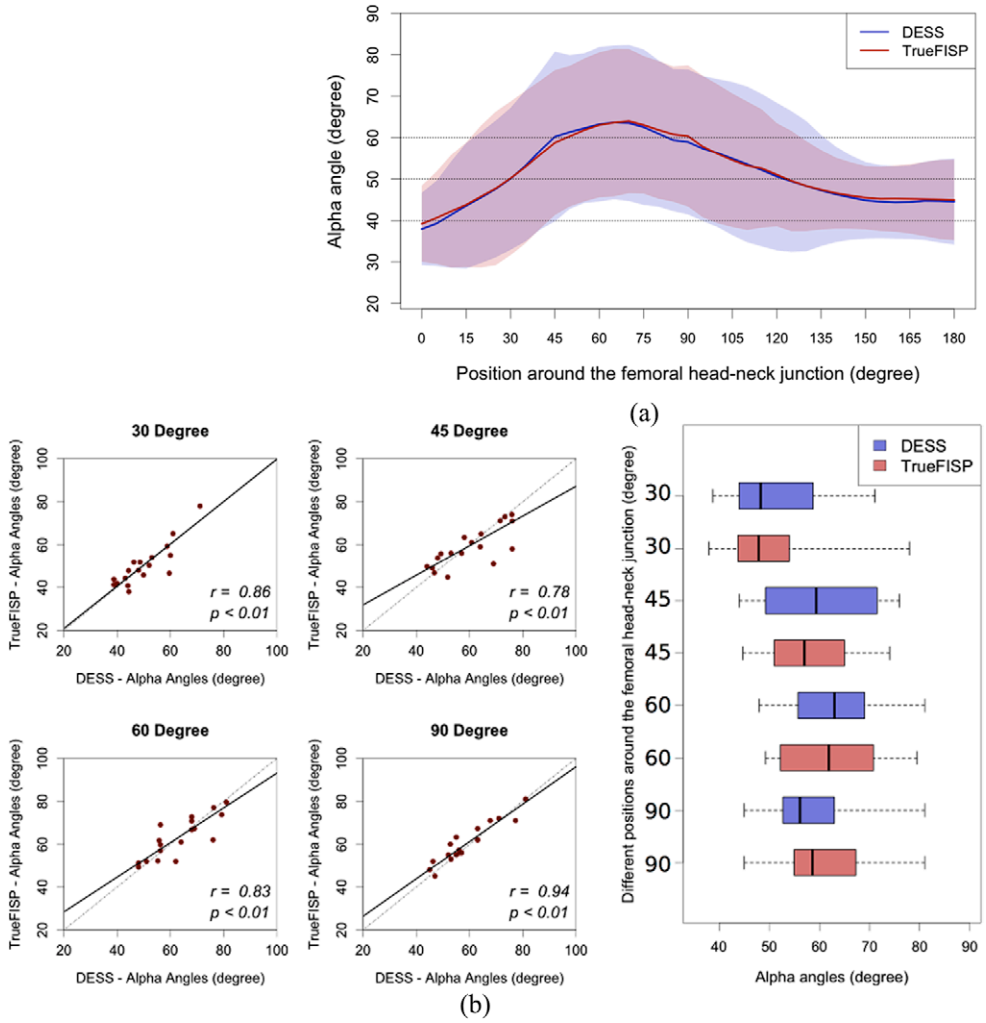

Figure 7. (a) Average alpha angle curves with regions of 95% CI across all positions 0°–180° of the FHN junction and (b) linear correlation plots and boxplots of alpha angles at four pre-selected positions (30°, 45°, 60°, 90°) in the upper anterior quadrant of the FHN junction in the reproducibility test between paired DESS and TrueFISP scans.

Rakhra *et al* 2009), there were very strong correlations ($r > 0.8$) between the manual (ground truth) and automatic alpha angle measures as derived from the ASM-based 3D segmentations of the proximal femur. Moreover, our method showed good reproducibility for automatic alpha angle measures derived from the paired DESS and TrueFISP images, which yielded strong correlations ($r > 0.78$) of alpha angles acquired across multiple sites in the upper anterior quadrant of the FHN junction (see figure 7(b)).

Alpha angles measured at one or two locations of the FHN junction in a traditional 2D manner have shown limited sensitivity for discrimination between asymptomatic and symptomatic (FAI) hips (Jung *et al* 2011, Sutter *et al* 2012). Recently, Lepage-Saucier *et al* (2014) found the ranges of anterosuperior and anterior alpha angles in asymtomatic hips exceeded

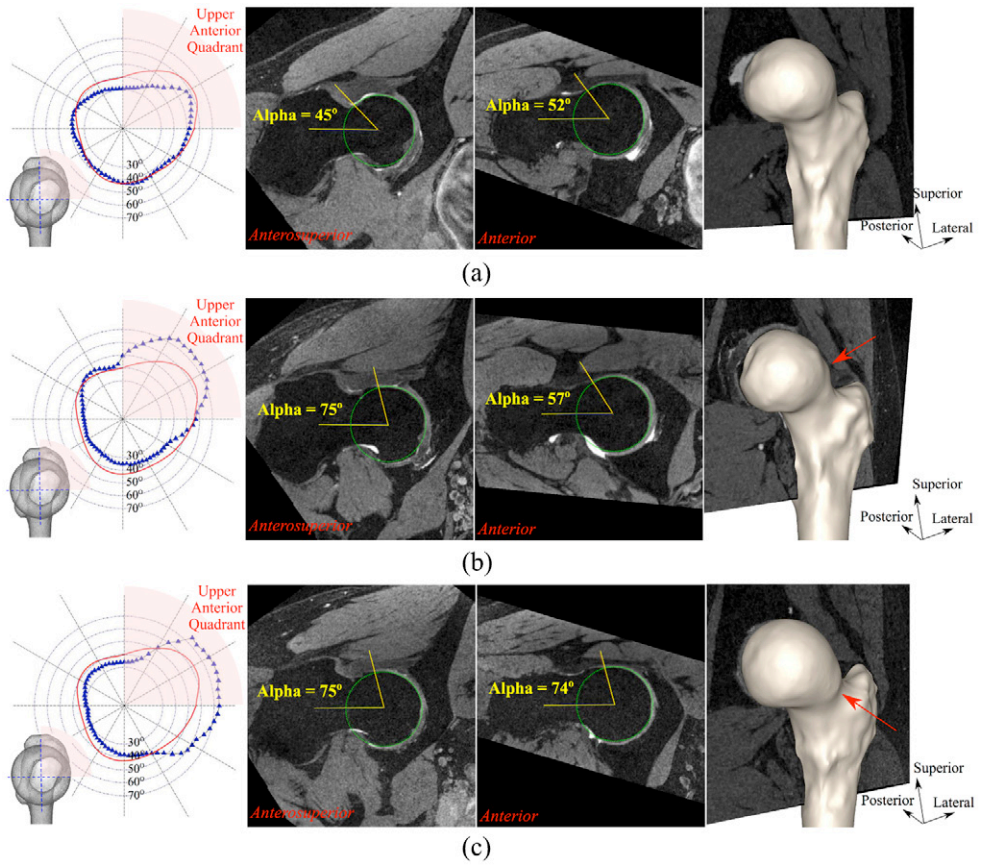

Figure 8. Example assessment results for hip joints having (a) smaller anterosuperior and anterior alpha angles, (b) a larger anterosuperior alpha angle, (c) larger anterosuperior and anterior alpha angles: (from left to right) polar plots of alpha angles (blue dots) around the FHN junction, anterosuperior radial slices, anterior radial slices and 3D bone models of the segmented proximal femur surfaces. The red circles in the alpha angle diagrams indicate the average alpha angle contour computed from the bilateral DESS images (i.e. 60 hips).

the 50°–60° cutoff thresholds for cam-type FAI. Our method offers the direct visualization and 360° measurement of the FHN junction on a patient-specific basis as shown in figure 8. It exploits the superiority of 3D analysis allowing detailed examination of alpha angle sizes and distribution characteristics (e.g. epicentre and extent of these osseous protrusions, see polar plots in figure 8) for assessing the full extent and shape of cam lesions. With 360° calculation of alpha angles around the FHN junction, the maximum alpha angle (red arrows in figure 8) can be determined, which can serve as the basis for further focused evaluation of the lesion as well as the damage to its surrounding soft tissues (e.g. the labrum and articular cartilage). Therefore, this fully automated approach offers the capacity to provide comprehensive 3D morphometric assessment and improved characterization of alpha angle data (e.g. the abnormal threshold, reference intervals in asymptomatic/symptomatic hips), for assistance in diagnosis and monitoring of cam-type FAI.

For the bilateral DESS images, manual measurements of alpha angles from auto-extracted radial slices at the anterosuperior and anterior positions of the FHN junction showed very high

intra- and inter-rater reliability (ICCs > 0.95). The excellent reliability of these ground truth measures was, in large part, attributed to the standardized, auto-extraction of the radial slices (see figure 2), which avoided the intra/inter-rater inconsistencies (subjective biases) associated with traditional manual image reformation processes. Although direct visualization of the auto-extracted 2D radial slices (figure 3(b)) is not necessary for the automated measurement of alpha angles from the current assessment scheme, all images are readily obtained to allow further evaluation or review by expert observers.

Our automatic approach is ideally suited for MR analyses of FHN alpha angles in both individual patients and in population-based investigations of asymptomatic (apparently healthy) and FAI cohorts. For the large range of alpha angles (41° to 88°) from the anterosuperior and anterior positions obtained in the current study, there was very favourable agreement between the fully automated and manual measures. The exceptionally robust performance of the automatic measurement approach using a 2D shape map of the femoral head for determining alpha angles across individuals with 'normal' values (e.g. <50–55° (Nötzli *et al* 2002, Nouh *et al* 2008)), 'high' values (60–70°) and 'very high' values (>70°) attests to the effectiveness of this method to analyse a wide variety of bone morphologies occurring at the anterosuperior and anterior positions of the FHN junction. Similarly, very strong correlations between the manual and automated alpha angle measures for the anterosuperior ($r = 0.84$) and anterior ($r = 0.92$) positions were obtained across these two different locations where typically the anterosuperior slice profile demonstrates a greater concavity of the FHN junction (figure 6).

The current work builds upon our studies into the morphometry of the osteochondral elements (e.g. bones and cartilages) of the human hip region focusing on the development of automated analysis to facilitate larger-scale research and clinical MR studies for pre- and early hip OA (Xia *et al* 2013, 2014, Chandra *et al* 2015c). Our proposed method provides reliable quantitative data on cam lesions, which has the potential to enhance the diagnosis and treatment of this pre-osteoarthritic condition aimed at reducing cartilage degeneration in the hip joint (Ganz *et al* 2003). To facilitate clinical application of the current work, future investigations involving fuller evaluation of the automated measurement method with larger subject cohorts with varied demographics (e.g. asymptomatic and symptomatic, males and females, different age groups) and clinical MR sequences (e.g. 2D or 3D fast spin-echo) would be beneficial. Similarly, further work to include and validate the automatic measurement of a suite of parameters such as the FHN offset (Tannast *et al* 2007), triangular index (Gosvig *et al* 2007) and 3D head-neck ratios (Masjedi *et al* 2013b) along with the alpha angle measures as validated in the current assessment scheme would enhance efforts targeting morphometric quantification of cam lesions. In addition, our automated assessment method can be readily extended in future work to provide simultaneous 3D measurements from the acetabulum for parallel analysis of pincer-type lesions in FAI (Tannast *et al* 2007, Dandachli *et al* 2012).

Acknowledgments

The research was supported by funding from the Australian Research Councils Linkage Projects scheme LP100200422.

References

Aliprandi A, Di Pietto F, Minafra P, Zappia M, Pozza S and Sconfienza L 2014 Femoro-acetabular impingement: what the general radiologist should know *Radiol. Med.* **119** 103–12

Audenaert E, Baelde N, Huysse W, Vigneron L and Pattyn C 2011 Development of a 3D detection method of cam deformities in femoroacetabular impingement *Skeletal Radiol.* **40** 921–7

Barton C, Salineros M, Rakhra K and Beaulé P 2011 Validity of the alpha angle measurement on plain radiographs in the evaluation of cam-type femoroacetabular impingement *Clin. Orthop. Relat. Res.* **469** 464–9

Beaulé P E, Zaragoza E, Motamedi K, Copelan N and Dorey F J 2005 3D computed tomography of the hip in the assessment of femoroacetabular impingement *J. Orthop. Res.* **23** 1286–92

Bedi A, Dolan M, Magennis E, Lipman J, Buly R and Kelly B T 2012 Computer-assisted modeling of osseous impingement and resection in femoroacetabular impingement *Arthroscopy* **28** 204–10

Bland J M and Altman D G 1986 Statistical methods for assessing agreement between two methods of clinical measurement *The Lancet* **327** 307–10

Chabanas L, LaVallee S, Tonetti J, Byrd T, Kelly B T and Larson C 2014 *Method and System of Automatic Determination of Geometric Elements Characterizing a Bone Deformation from 3D Image* (Washington, DC: US Patent and Trademark Office: Google Patents)

Chandra S S *et al* 2015a A simple framework for the rapid development of biomedical imaging applications *IEEE Trans. Biomed. Eng.* submitted

Chandra S S, Fripp J, Neubert A, Shen K-K, Engstrom C and Crozier S 2015b Focused shape visualisation via the robust shape modelling toolkit *IEEE Trans. Vis. Comput. Graphics* submitted

Chandra S S, Surowiec R, Ho C, Xia Y, Engstrom C, Crozier S and Fripp J 2015c Automated analysis of hip joint cartilage combining MR T2 and 3D fast-spin-echo images *Magn. Reson. Med.* at press

Chandra S S, Xia Y, Engstrom C, Crozier S, Schwarz R and Fripp J 2014 Focused shape models for hip joint segmentation in 3D magnetic resonance images *Med. Image Anal.* **18** 567–78

Clohisy J, Carlisle J, Trousdale R, Kim Y-J, Beaule P, Morgan P, Steger-May K, Schoenecker P and Millis M 2009 Radiographic evaluation of the hip has limited reliability *Clin. Orthop. Relat. Res.* **467** 666–75

Commandeur F, Velut J and Acosta O 2011 A VTK algorithm for the computation of the Hausdorff distance *VTK J.* **839** (http://hdl.handle.net/10380/3322)

Dai M, Newman T S and Cao C 2007 Least-squares-based fitting of paraboloids *Pattern Recognit.* **40** 504–15

Dandachli W, Najefi A, Iranpour F, Lenihan J, Hart A and Cobb J 2012 Quantifying the contribution of pincer deformity to femoro-acetabular impingement using 3D computerised tomography *Skeletal Radiol.* **41** 1295–300

Dice L R 1945 Measures of the amount of ecologic association between species *Ecology* **26** 297–302

Dudda M, Albers C, Mamisch T, Werlen S and Beck M 2009 Do normal radiographs exclude asphericity of the femoral head-neck junction? *Clin. Orthop. Relat. Res.* **467** 651–9

Fischler M A and Bolles R C 1981 Random sample consensus: a paradigm for model fitting with applications to image analysis and automated cartography *Commun. ACM* **24** 381–95

Ganz R, Parvizi J, Beck M, Leunig M, Nötzli H and Siebenrock K A 2003 Femoroacetabular impingement: a cause for osteoarthritis of the hip *Clin. Orthop. Relat. Res.* **417** 112–20 (PMID: 14646708)

Gerig G, Jomier M and Chakos M 2001 Valmet: a new validation tool for assessing and improving 3D object segmentation *Medical Image Computing and Computer-Assisted Intervention–MICCAI 2001*(Berlin: Springer) pp 516–23

Gosvig K K, Jacobsen S, Palm H, Sonne-Holm S and Magnusson E 2007 A new radiological index for assessing asphericity of the femoral head in cam impingement *J. Bone Joint Surg. Br.* **89-B** 1309–16

Harris M D, Datar M, Whitaker R T, Jurrus E R, Peters C L and Anderson A E 2013b Statistical shape modeling of cam femoroacetabular impingement *J. Orthop. Res.* **31** 1620–6

Harris M D, Kapron A L, Peters C L and Anderson A E 2014 Correlations between the alpha angle and femoral head asphericity: implications and recommendations for the diagnosis of cam femoroacetabular impingement *Eur. J. Radiol.* **83** 788–96

Harris M D, Reese S P, Peters C L, Weiss J A and Anderson A E 2013a Three-dimensional quantification of femoral head shape in controls and patients with cam-type femoroacetabular impingement *Ann. Biomed. Eng.* **41** 1162–71

Jung K A, Restrepo C, Hellman M, AbdelSalam H, Morrison W and Parvizi J 2011 The prevalence of cam-type femoroacetabular deformity in asymptomatic adults *J. Bone Joint Surg. Br.* **93-B** 1303–7

Kang X, Zhang H, Garbuz D, Wilson D and Hodgson A 2013 Preliminary evaluation of an MRI-based technique for displaying and quantifying bony deformities in cam-type femoroacetabular impingement *Int. J. CARS* **8** 967–75

Lepage-Saucier M, Thiéry C, Larbi A, Lecouvet F, Vande Berg B and Omoumi P 2014 Femoroacetabular impingement: normal values of the quantitative morphometric parameters in asymptomatic hips *Eur. Radiol.* **24** 1707–14

Masjedi M, Harris S J, Davda K and Cobb J P 2013a Mathematical representation of the normal proximal human femur: application in planning of cam hip surgery *Proc. Inst. Mech. Eng.* **227** 421–7

Masjedi M, Marquardt C S, Drummond I M, Harris S J and Cobb J P 2013b Cam type femoro-acetabular impingement: quantifying the diagnosis using three-dimensional head-neck ratios *Skeletal Radiol.* **42** 329–33

Meyer D C, Beck M, Ellis T, Ganz R and Leunig M 2006 Comparison of six radiographic projections to assess femoral head/neck asphericity *Clin. Orthop. Relat. Res.* **445** 181–5

Nishii T, Sugano N, Sato Y, Tanaka H, Miki H and Yoshikawa H 2004 3D distribution of acetabular cartilage thickness in patients with hip dysplasia: a fully automated computational analysis of MR imaging *Osteoarthritis Cartilage* **12** 650–7

Nötzli H P, Wyss T F, Stoecklin C H, Schmid M R, Treiber K and Hodler J 2002 The contour of the femoral head-neck junction as a predictor for the risk of anterior impingement *J. Bone Joint Surg. Br.* **84** 556–60

Nouh M R, Schweitzer M E, Rybak L and Cohen J 2008 Femoroacetabular impingement: can the alpha angle be estimated? *Am. J. Roentgenol.* **190** 1260–2

Pfirrmann C W, Mengiardi B, Dora C, Kalberer F, Zanetti M and Hodler J 2006 Cam and pincer femoroacetabular impingement: characteristic MR arthrographic findings in 50 patients *Radiology* **240** 778–85

Rakhra K, Sheikh A, Allen D and Beaulé P 2009 Comparison of MRI alpha angle measurement planes in femoroacetabular impingement *Clin. Orthop. Relat. Res.* **467** 660–5

Sholukha V, Chapman T, Salvia P, Moiseev F, Euran F, Rooze M and Van Sint Jan S 2011 Femur shape prediction by multiple regression based on quadric surface fitting *J. Biomech.* **44** 712–8

Streit J J, Fortun C M and Salata M J 2012 Cam-type femoroacetabular impingement *Oper. Tech. Sports Med.* **20** 295–300

Sutter R, Dietrich T J, Zingg P O and Pfirrmann C W A 2012 How useful is the alpha angle for discriminating between symptomatic patients with cam-type femoroacetabular impingement and asymptomatic volunteers? *Radiology* **264** 514–21

Tannast M, Goricki D, Beck M, Murphy S B and Siebenrock K A 2008 Hip damage occurs at the zone of femoroacetabular impingement *Clin. Orthop. Relat. Res.* **466** 273–80

Tannast M, Siebenrock K A and Anderson S E 2007 Femoroacetabular impingement: radiographic diagnosis—what the radiologist should know *Am. J. Roentgenol.* **188** 1540–52

Wagner S, Hofstetter W, Chiquet M, Mainil-Varlet P, Stauffer E, Ganz R and Siebenrock K A 2003 Early osteoarthritic changes of human femoral head cartilage subsequent to femoro-acetabular impingement *Osteoarthritis Cartilage* **11** 508–18

Xia Y, Chandra S S, Engstrom C, Strudwick M W, Crozier S and Fripp J 2014 Automatic hip cartilage segmentation from 3D MR images using arc-weighted graph searching *Phys. Med. Biol.* **59** 7245

Xia Y, Fripp J, Chandra S S, Schwarz R, Engstrom C and Crozier S 2013 Automated bone segmentation from large field of view 3D MR images of the hip joint *Phys. Med. Biol.* **58** 7375

Zilkens C, Miese F, Krauspe R and Bittersohl B 2013 Symptomatic femoroacetabular impingement: does the offset decrease correlate with cartilage damage? A pilot study *Clin. Orthop. Relat. Res.* **471** 2173–82